JOURNAL OF COMPUTATIONAL PHYSICS **124,** 301–308 (1996)
ARTICLE NO. 0061

A New Finite Variable Difference Method with Application to Locally Exact Numerical Scheme

KATSUHIRO SAKAI

Saitama Institute of Technology, Department of Electrical Engineering, 1690 Fusaiji, Okabecho, Osatogun, Saitama 369-02, Japan

Received March 22, 1994; revised July 14, 1995

A new finite variable difference method (FVDM) on finite differencing is presented. The essence of this method consists in determining the optimum spatial difference such that the total variance of the solution is a minimum under the condition that characteristic roots of the resulting difference equation are always nonnegative to ensure the numerical stability. The present FVDM is applied to the locally exact numerical scheme (LENS). The optimum spatial difference of the LENS is derived in terms of local mesh Reynolds numbers. By using this optimum spatial difference the numerical accuracy of the LENS for the linear convection–diffusion equations is increased without numerical oscillations for all mesh Reynolds numbers. The present study suggests that an optimum spatial difference from the viewpoint of numerical stability and accuracy exists according to the numerical schemes.

1. INTRODUCTION

So far several high-order numerical schemes with constant difference coefficients for the convection term in transport equations have been developed [1–5], based on polynomial differencing. However, these linear high-order schemes tend to suffer from the Godunov theorem [6] regarding the monotonicity of numerical solutions. Namely, numerical solutions with linear high-order schemes may happen to show unphysical oscillations (numerical oscillations) when mesh Reynolds or Peclet numbers exceed a critical value (approximately 2). To cope with this instability problem, nonlinear schemes preserving monotonicity such as the FCT [7] and FRAM [8] techniques to suppress the local oscillations, and the TVD schemes [9, 10] with a numerical flux limiter function have been proposed.

On the other hand, the concept of locally exact numerical differencing was introduced by Allen and Southwell [11], upon which numerical schemes involving three points in a one-dimensional field were developed [11, 12]. Beyond these, the LSUDS (Leonard super upwind scheme) [13] and the LECUSSO (locally exact consistent upwind scheme of second order) [14] were proposed. The LECUSSO and LSUDS schemes use four and five base points in one-dimension, respectively. Versions of the LECUSSO scheme have been proposed which are formulated in a conservation form for uniform mesh size grids [15] and for nonuniform mesh sizes [16]. Those locally exact schemes are characterized by determining the difference coefficients so that the resulting difference equation satisfies the exact solution of the convection–diffusion equation with constant coefficients. The difference coefficients depend on local velocities and these locally exact schemes are nonlinear, resulting in their possessing the possibility of being free from the Godonuv theorem.

Those locally exact schemes have been extended to transport equations with absorption [17, 18] and source terms [19]. The present author proposed the LENS (locally exact numerical scheme) [20], including the sources and absorption, in which the sources are not constant but locally polynomial, and the spatial distribution of the coefficients of the transport equation in a control volume is taken into consideration, based on a two-region model [21]. The LENS shows [22] stable and accurate solutions for transport equations with source terms, as compared with the conventional high-order schemes such as the LECUSSO and QUICK schemes.

When we construct numerical schemes, numerical stability and good accuracy are required for the numerical schemes. Regarding the numerical stability, the stability study of difference schemes for one-dimensional convection–diffusion equations on the basis of the characteristic equation roots was performed by Degtyarev *et al.* [23]. Independently, the present author performed the stability analysis for the LECUSSO scheme in uniform [16] and nonuniform mesh sizes [24] by using a characteristic polynomial method, in which the necessary and sufficient conditions against numerical oscillations for steady state problems are that all the roots of the characteristic equations for the difference equations be nonnegative. Regarding the numerical accuracy, it has been so far defined as the lowest order of the truncation errors of the difference equations. However, in case the numerical solutions involve the numerical oscillations the conventional definition for the accuracy is not reasonable but the variance defined as the total deviation from its exact solution, if any, or its reference solution which is obtained with a fine mesh grid, is reasonable.

0021-9991/96 $18.00

On the other hand, in the conventional FDM (finite difference method), a spatial mesh increment Δx has been used as the spatial difference for the discretization. In this paper a new finite variable difference method FVDM is proposed, in which a variable spatial difference, instead of the conventional Δx is adopted for the discretization of the convection term. The present FVDM is applied to the LENS based on the locally exact numerical differencing. The variable spatial difference is optimized from the viewpoint of numerical stability and accuracy. Namely, an optimum spatial difference for the LENS is determined in terms of the mesh Reynolds number such that at first the characteristic roots of the resulting difference equation are to be always nonnegative to assure the numerical stability for any mesh Reynolds number and, then, the variance of the numerical solution is a minimum. Thus the optimized LENS with the optimum spatial difference has been examined through numerical experiments.

2. MATHEMATICAL FORMULATION

2.1. Transport Equations

We consider the one-dimensional, linear convection–diffusion equation,

$$\frac{d^2\phi}{dx^2} - R\frac{d\phi}{dx} = 0, \tag{1}$$

where ϕ is the transported quantity and x denotes the Cartesian space coordinate. R is the ratio of the transporting velocity v to the diffusion parameter ν such as the kinematic viscosity.

Here we assume R is constant. Then the general solution for Eq. (1) is given as

$$\phi = C_1 \exp[Rx] + C_2, \tag{2}$$

where C_1 and C_2 are constants determined by the boundary conditions, but here they are not necessary to be specified, as explained later.

2.2. Difference Formula

We approximate the convection term in Eq. (1) using the present FVDM as follows:

$$\frac{d\phi}{dx} = \frac{(\phi_{i+p} - \phi_{i-p})}{2p\,\Delta x}. \tag{3}$$

Here ϕ_{i+p} and ϕ_{i-p} are the transported quantities at $x = x_i + p\,\Delta x$, and $x = x_i - p\,\Delta x$, respectively as shown in Fig. 1 with the uniform mesh size Δx. In Eq. (3), $p = \frac{1}{2}$ corresponds to the conventional FDM. Here we consider $0 < p < 1$. Then ϕ_{i+p} and ϕ_{i-p} for $v > 0$ are approximated by the following expressions based on the upwind differencing:

$$\phi_{i-p} = a\,\phi_i + b\phi_{i-1} + c\phi_{i-2}, \tag{4a}$$

$$\phi_{i+p} = a'\phi_{i+1} + b'\phi_i + c'\phi_{i-1}. \tag{4b}$$

In Eqs. (3) and (4), if p is larger than $\frac{1}{2}$, the upwinding weight becomes large. Hence p means of a kind of upwinding parameter. Next we determine the difference coefficients a, b, c, a', b', and c'.

2.3. Optimized LENS Scheme

2.3.1. *Difference Coefficients*

We impose the condition that Eqs. (4a) and (4b) satisfy identically the exact solution Eq. (2) of Eq. (1) for arbitrary values of C_1 and C_2. According to the mathematical procedures in Ref. (20) or (22), we get the following matrix equations for the difference coefficients:

$$[M]\begin{bmatrix} a \\ b \\ c \end{bmatrix} = \begin{bmatrix} 1 \\ x_{i-p} \\ \exp[Rx_{i-p}] \end{bmatrix}, \tag{5}$$

$$[N]\begin{bmatrix} a' \\ b' \\ c' \end{bmatrix} = \begin{bmatrix} 1 \\ x_{i+p} \\ \exp[Rx_{i+p}] \end{bmatrix}, \tag{6}$$

where

$$[M] = \begin{bmatrix} 1 & 1 & 1 \\ x_i & x_{i-1} & x_{i-2} \\ \exp[Rx_i] & \exp[Rx_{i-1}] & \exp[Rx_{i-2}] \end{bmatrix}, \tag{7}$$

$$[N] = \begin{bmatrix} 1 & 1 & 1 \\ x_{i+1} & x_i & x_{i-1} \\ \exp[Rx_{i+1}] & \exp[Rx_i] & \exp[Rx_{i-1}] \end{bmatrix}, \tag{8}$$

If p is given in the above equations, we obtain a, b, c, a', b', and c' from Eqs. (5)–(8). Next we will determine the optimum value of p from the viewpoints of numerical stability and accuracy.

2.3.2. *Characteristic Equation*

Discretizing the convection and diffusion terms in Eq. (1) with Eq. (3) and the second-order central scheme, respectively, we have

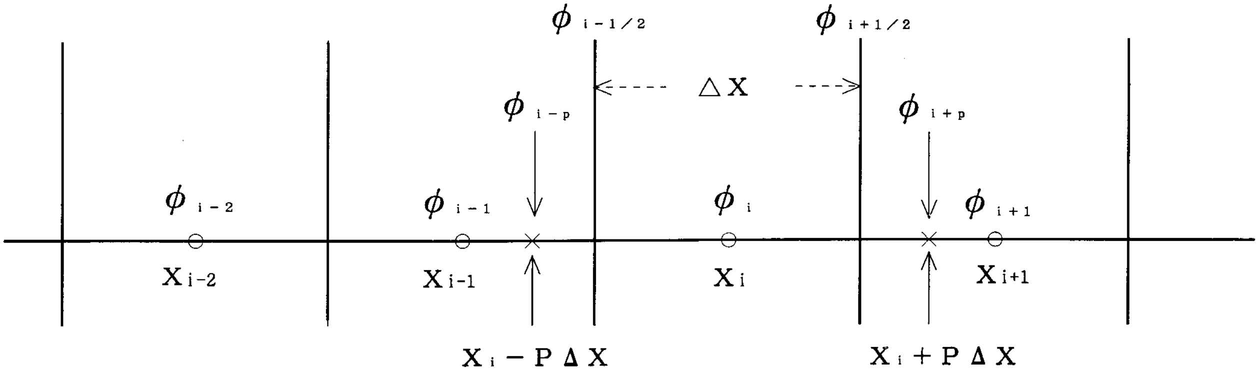

FIG. 1. Finite spatial difference in FVDM.

$$\begin{aligned}(\phi_{i+1} - 2\phi_i + \phi_{i-1})& \\ -(Rm/2p)\{[a'\phi_{i+1} + b'\phi_i + c'\phi_{i-1}]& \\ -[a\phi_i + b\phi_{i-1} + c\phi_{i-2}]\} = 0,&\end{aligned} \tag{9}$$

with $Rm = R\Delta x$ (mesh Reynolds number) in a uniform mesh size grid. Rearranging the above equation yields the difference equation

$$A\phi_{i+1} + B\phi_i + C\phi_{i-1} + D\phi_{i-2} = 0, \tag{10}$$

where

$$\begin{aligned}A &\equiv 1 - (Rm/2p)a', & B &\equiv -[2 + (Rm/2p)(b' - a)],\\ C &\equiv 1 - (Rm/2p)(c' - b), & D &\equiv (Rm/2p)c.\end{aligned} \tag{11}$$

Equation (10) has an exact solution

$$\phi_i = \alpha(\lambda_1)^i + \beta(\lambda_2)^i + \gamma(\lambda_3)^i, \tag{12}$$

where α, β, and γ are constants determined by the boundary conditions. In Eq. (12), λ_1, λ_2, and λ_3 are the roots of the characteristic equation

$$A\lambda^3 + B\lambda^2 + C\lambda + D = 0. \tag{13}$$

Since $a + b + c = 1$ and $a' + b' + c' = 1$ hold in Eqs. (5)–(8), from Eq. (11) we get the relation

$$\begin{aligned}A + B + C + D = -(Rm/2p)&\\ [(a' + b' + c') - (a + b + c)]&\\ = 0.&\end{aligned} \tag{14}$$

Hence Eq. (13) has the root $\lambda_1 = 1$ and can be factorized as

$$\begin{aligned}(\lambda - 1)\{[1 - (Rm/2p)a']\lambda^2&\\ - [1 + (Rm/2p)(1 - c' - a)]\lambda - (Rm/2p)c\} = 0.&\end{aligned} \tag{15}$$

From this equation, we obtain the other two roots

$$\lambda_2 = \frac{1 + (Rm/2p)(1 - c' - a) + \sqrt{\Sigma}}{2[1 - (Rm/2p)a']}, \tag{16a}$$

$$\lambda_3 = \frac{1 + (Rm/2p)(1 - c' - a) - \sqrt{\Sigma}}{2[1 - (Rm/2p)a']}, \tag{16b}$$

where

$$\begin{aligned}\Sigma \equiv [1 + (Rm/2p)(1 - c' - a)]^2&\\ + 4[1 - (Rm/2p)a'](Rm/2p)c.&\end{aligned} \tag{17}$$

2.3.3. *Stability Condition*

Since the numerical oscillation is due to the behavior of an exact solution of the difference equation, and not the numerical instability due to an accumulation of roundoff errors, we examine the behavior of Eq. (12). Even if one of the roots (λ_1, λ_2, λ_3) is negative, ϕ_i oscillates with the wave length of $2\Delta x$ as seen in Eq. (12). Therefore, the necessary and sufficient condition for the smooth solution is that all the characteristic roots (λ_1, λ_2, λ_3) are real and nonnegative [16, 24]. Namely, we have the stability condition:

$$\Sigma \geqq 0, \quad \lambda_1 \geqq 0, \quad \lambda_2 \geqq 0, \quad \lambda_3 \geqq 0. \tag{18}$$

We numerically examine the dependence of the characteristic roots on p ($0.1 \leqq p \leqq 1$) for ($0.1 \leqq Rm \leqq 1000$). Here we consider Rm of up to 1000, since Rm reaches a value of several hundreds in usual hydraulic calculations. The first stability condition $\Sigma \geqq 0$ is always fulfilled for

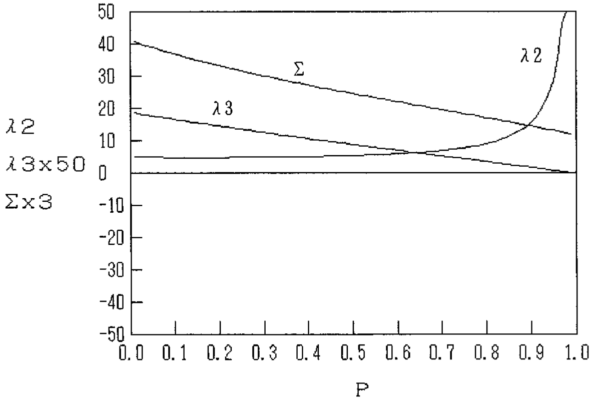

FIG. 2. Dependence of λ_2, λ_3, and Σ on p at $Rm = 2$.

any p and Rm. Figures 2 and 3 show the dependence of Σ, λ_2, and λ_3 on p at $Rm = 2$ and $Rm = 10$, respectively. From these figures, we can see that both λ_2 and λ_3 are positive for all p under consideration in the case of $Rm = 2$, while in the case of $Rm = 10$ an asymptote ($p = p_a$) for λ_2 exists, and λ_2 is negative for $p > p_a$. At $p = \frac{1}{2}$ both λ_2 and λ_3 are always positive. This is the reason why the original LENS with $p = \frac{1}{2}$ shows stable solutions.

The asymptote ($p = p_a$) for λ_2 occurs when the denominator of Eq. (16) is zero. Namely, the equation to determine p_a is

$$1 - (Rm/2p_a)a'(p_a, Rm) = 0, \tag{19}$$

where the notation $a'(p_a, Rm)$ is used, since the coefficient a' involves p and Rm as parameters. When p approaches p_a, the numerator of λ_3, given by Eq. (16b) approaches zero. Hence λ_3 varies continuously even in the vicinity of $p = p_a$. A critical value *Rmc,* where λ_2 can be negative for Rm greater than Rmc, is given by Eq. (19) with $p_a = 1.0$, which is the maximum value of p. Namely, the equation to determine Rmc is

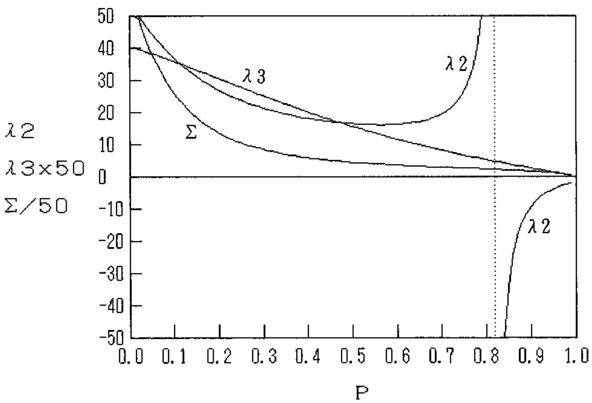

FIG. 3. Dependence of λ_2, λ_3, and Σ on p at $Rm = 10$.

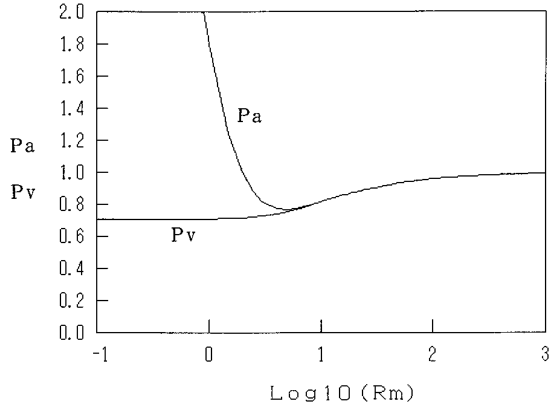

FIG. 4. Dependence of p_a and p_v on Rm.

$$1 - (Rmc/2)a'(1.0, Rmc) = 0. \tag{20}$$

At first we determine Rmc by numerically solving Eq. (20). We obtain exactly $Rmc = 2$. Then we numerically solve Eq. (19) for $Rm > Rmc$ and obtain the asymptote p_a in terms of Rm. Figure 4 and Table I show the dependence of p_a on Rm. If p exceeds p_a, λ_2 becomes negative and the solution Eq. (12) oscillates. Therefore, to ensure the numerical stability, p must be

$$(\text{for } Rm \leqq 2) \quad \text{arbitrary value of } 0 < p < 1, \tag{21a}$$

TABLE I

Dependence of p_a and p_o on Rm

Rm	$p_a = F(Rm)$	p_o	
0.1	10.000000	0.707140	$G(Rm)$
0.5	3.626053	0.707840	
1.0	1.799491	0.710010	
1.5	1.242192	0.713500	
2.0	1.000000	0.718160	
3.0	0.819471	0.730170	
4.0	0.774213	0.744290	
6.0	0.776796	0.773220	
8.0	0.798949	0.798500	
10.0	0.819149	0.819090	
12.0	0.835739	0.835730	
13.0	0.842868	0.842860	
14.0	0.849344	0.849343	Eq. (24b)
15.0	0.855349	0.855348	
17.0	0.865625	0.865625	
20.0	0.878387	0.878387	Eq. (24c)
25.0	0.894512	0.894512	
30.0	0.906458	0.906458	
50.0	0.934263	0.934263	
75.0	0.951006	0.951006	
100.	0.960477	0.960477	
500.	0.988935	0.988935	
700.	0.991620	0.991620	
1000.	0.993779	0.993779	

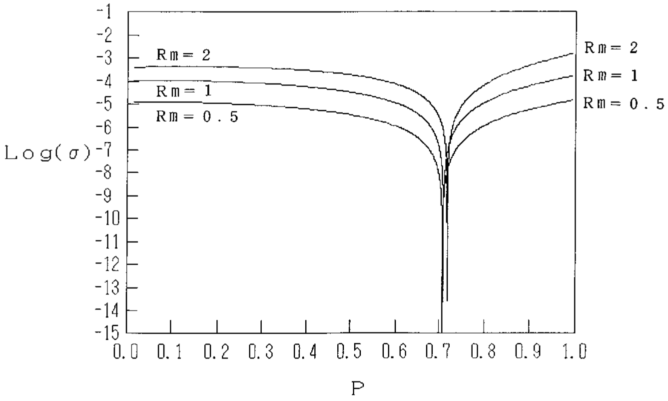

FIG. 5. Dependence of variance σ on p at small Rm.

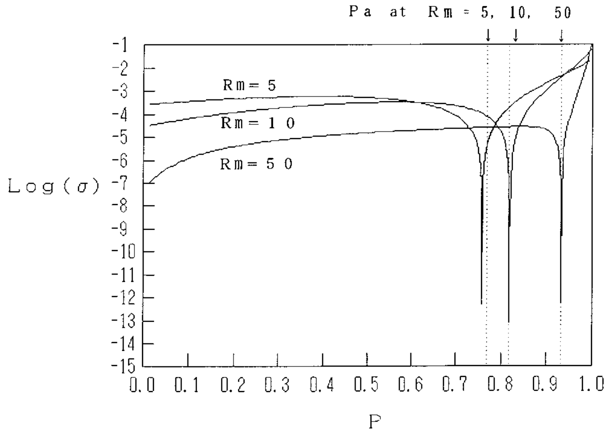

FIG. 6. Dependence of variance σ on p at middle Rm.

$$(\text{for } Rm > 2) \quad 0 < p < p_a = F(Rm). \tag{21b}$$

From Table I we can construct the function $F(Rm)$ by fitting a regression line such as the least squares method, when necessary.

2.3.4. *Variance*

Here we evaluate the dependence of the variance of numerical solutions on p. We define the variance σ as

$$\sigma \equiv \frac{1}{n} \sum_{i=1}^{n} [\phi_i - \phi_e(x_i)]^2, \tag{22}$$

where n is the total mesh number, ϕ_i and $\phi_e(x_i)$ represent the numerical solution and the exact solution at the mesh number i, respectively.

To evaluate σ we perform typical calculations in one-dimensional geometry with the uniform mesh $\Delta x = 1/n$, in which the total mesh number n and total computational length are 15 and 1, respectively. The boundary values at $x = 0$ and $x = 1$ are set $\phi(0) = 1$ and $\phi(1) = 0$. This calculation with a Dirichlet outflow boundary condition is a difficult problem since it generates a thin boundary layer near the exit ($x = 1$) as the mesh Reynolds numbers increase.

We perform survey calculations with double precision by using the increment $\Delta p = 10^{-6}$ over $0 < p < 1$, and find the value of p which minimizes σ (we denote p_v). Figures 5, 6, and 7 show the dependence of σ on p for $Rm \leqq 2$, for $5 \leqq Rm \leqq 100$, and for $500 \leqq Rm \leqq 1000$, respectively. It is noticeable that σ in these figures significantly decreases in the vicinity of p_v. We can see in Fig. 5 that p_v exists around 0.71 for $Rm \leqq 2$. In Figs. 6 and 7, where the asymptote for λ_2 is also shown, p_v for $Rm = 5$ exists at p slightly smaller than p_a, while p_v approaches p_a as Rm increases and it becomes almost equal to p_a at Rm greater than about 10. The dependence of p_v on Rm is shown in Fig. 4, together with p_a, from which the mutual relation between p_v and p_a can be seen.

According to the above survey calculations, we construct the correlation equation of p_v with respect to Rm:

$$(\text{for } 0 < Rm \leqq 14) \quad p_v = G(Rm), \tag{23a}$$

$$(\text{for } 14 \leqq Rm \leqq 20) \quad p_v = F(Rm) - 10^{-6}(20 - Rm)/6, \tag{23b}$$

$$(\text{for } 20 \leqq Rm) \quad p_v = F(Rm). \tag{23c}$$

The function $G(Rm)$ for Rm less than 14 is shown as p_v in Fig. 4 and as p_o in Table I.

The other calculations with the total mesh number $n = 20$ were performed to check the dependence of p_v on n, but p_v was the same as Eq. (23). Hence the value of p to minimize σ hardly depends on n at least greater than 15.

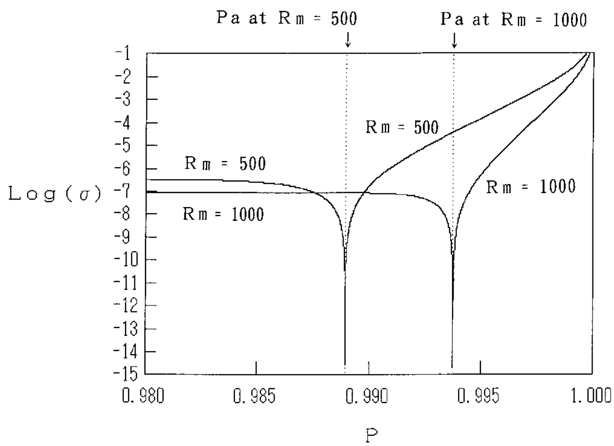

FIG. 7. Dependence of variance σ on p at large Rm.

2.3.5. *Optimum Value of p*

In order to optimize the numerical scheme, we initially require that the roots of the characteristic equation of the resulting difference equation must be nonnegative to ensure the numerical stability for any mesh Reynolds number under consideration ($0.1 \leqq Rm \leqq 1000$). Next we require that the variance of the numerical solution is a minimum under the stability condition.

In the previous section, the value of p_v to minimize the variance σ is always smaller than or equal to $p_a = F(Rm)$. Namely, p_v given by Eq. (23) satisfies the stability condition given by Eq. (21), except where p_v just equals p_a for Rm greater than 20. Although p_a for $Rm \geqq 20$ is the boundary between stable and unstable domains, the solutions with $p = p_a$ were still stable according to numerical experiments. Accordingly, the optimum p (we denote p_o) to fulfill the above two requirements (stability and accuracy) is

$$(\text{for } 0 < Rm \leqq 14) \quad p_o = G(Rm), \tag{24a}$$

$$(\text{for } 14 \leqq Rm \leqq 20) \quad p_o = F(Rm) - 10^{-6}(20 - Rm)/6, \tag{24b}$$

$$(\text{for } 20 \leqq Rm) \quad p_o = F(Rm). \tag{24c}$$

Table I shows the dependence of p_o on Rm, together with p_a.

From Fig. 4 and Table I, an interesting result is found that the optimization of the LENS from the viewpoint of numerical stability and accuracy for large mesh Reynolds numbers greater than about 10 is achieved when a root of the characteristic equation for the resulting difference equation approaches its asymptote, namely when the characteristic roots have poles.

3. TEST CALCULATIONS AND DISCUSSION

First, we compare the exact solution with the numerical solutions by using the original LENS with $p = \frac{1}{2}$ and the optimized LENS scheme with $p = p_o$ given by Eq. (24). The computational conditions are the same as in the above survey calculations with the total mesh number $n = 10$. Table II shows the comparison of those two solutions at $Rm = 1$ and 100. It is remarkable that the optimized LENS predicts the exact solution within five significant figures, even with the small mesh number $n = 10$. Especially the variance at $Rm = 100$ is quite small and the numerical accuracy, based on the total deviation from the analytical solution, turns out to be highly increased.

Next it is interesting whether p_o, given by Eq. (24), evaluated on the convection–diffusion equation without absorption and source terms, is effective for other types of transport equations. Here we consider the transport equation with absorption and source terms such as

TABLE II

Comparison of Numerical Solutions with the Analytical Solution

I	Exact solution	Original	Optimized
Case a, $Rm = 1.00$, optimum $p = 0.71001$			
1	1.00000	1.00000	1.00000
2	0.99992	0.99992	0.99992
3	0.99971	0.99964	0.99971
4	0.99913	0.99890	0.99913
5	0.99757	0.99697	0.99757
6	0.99331	0.99191	0.99331
7	0.98173	0.97868	0.98173
8	0.95026	0.94410	0.95026
9	0.86470	0.85373	0.86470
10	0.63215	0.61749	0.63215
11	0.00000	0.00000	0.00000
	Variance σ	3.498×10^{-5}	2.482×10^{-14}
Case b, $Rm = 100.0$, optimum $p = 0.960477$			
1	1.00000	1.00000	1.00000
2	1.00000	1.00000	1.00000
3	1.00000	1.00000	1.00000
4	1.00000	1.00000	1.00000
5	1.00000	1.00000	1.00000
6	1.00000	1.00000	1.00000
7	1.00000	1.00000	1.00000
8	1.00000	1.00000	1.00000
9	1.00000	1.00000	1.00000
10	1.00000	0.99336	1.00000
11	0.00000	0.00000	0.00000
	Variance σ	4.005×10^{-5}	8.715×10^{-22}

$$\frac{d^2\phi}{dx^2} - R\frac{d\phi}{dx} - S\phi + Q = 0, \tag{25}$$

where S and Q are the intensity of the absorption and source, respectively, and $Q = Q_0(x - 0.5)^2$. The exact

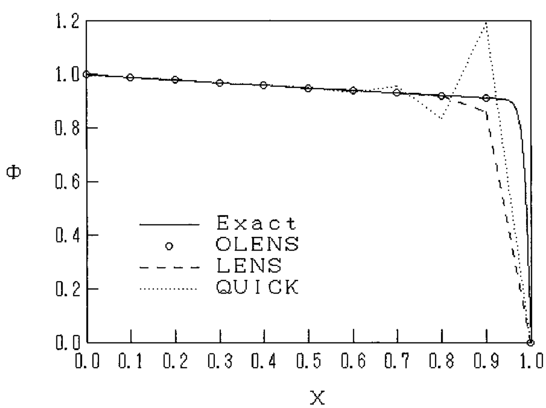

FIG. 8. Comparison of solutions with $Rm = 10$, $S = 10$, and $Q_0 = 1$.

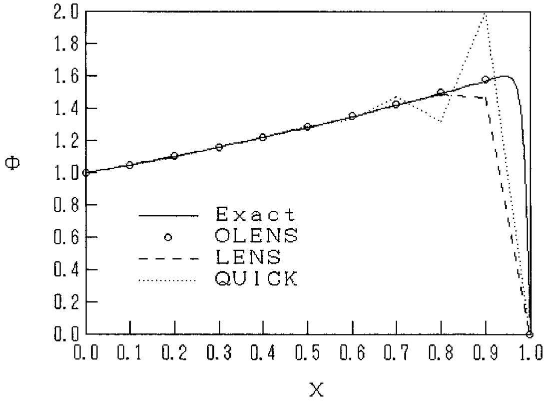

FIG. 9. Comparison of solutions with $Rm = 10$, $S = -50$, and $Q_0 = 1$.

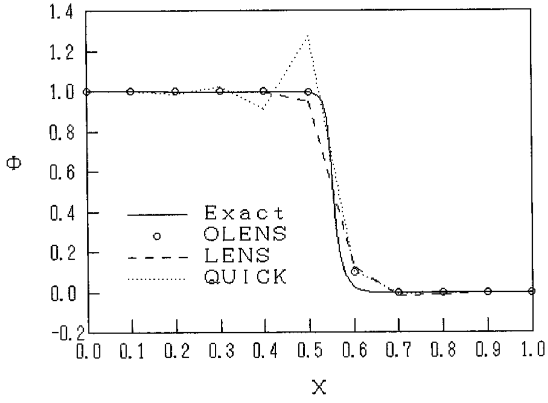

FIG. 11. Comparison of solutions with $Rm = 10$ and $S(x) = 10^4$ $(0.55 \leqq x \leqq 1)$.

solution of Eq. (25) is shown in Ref. (20). We solve Eq. (25) under the same computational conditions that were used in the first test calculations.

Figures 8, 9, and 10 show the comparison of solutions with ($Rm = 10$, $S = 10$, $Q_0 = 1$), ($Rm = 10$, $S = -50$, $Q_0 = 1$), and ($Rm = 100$, $S = 1000$, $Q_0 = 10$), respectively, together with the solutions by the QUICK scheme. In these figures, OLENS means the optimized LENS with the optimum spatial difference parameter p_o given by Eq. (24). The solutions with this optimized scheme are in good agreement with the exact solution at the mesh points without oscillations, while the solutions with the QUICK scheme show numerical oscillations.

In the above test calculations, the steep gradients of ϕ exist near the exit boundary ($x = 1$), where the ϕ just downstream from the steep gradient is not calculated but is given as the boundary condition. Hence we solve Eq. (25) with a strong absorption in the half-computational region ($0.55 \leqq x \leqq 1$) and without absorption in the other region ($0 \leqq x < 0.55$), using the same Dirichlet boundary condition ($\phi(0) = 1$, $\phi(1) = 0$) as the first test calculations. The analytical solution is easily obtained by imposing the continuous conditions of ϕ and $d\phi/dx$ at the inner boundary ($x = 0.55$). Figures 11 and 12 show the comparison of solutions with $S(x) = 10^4$ for $0.55 \leqq x \leqq 1$ at $Rm = 10$, and $S(x) = 10^6$ for $0.55 \leqq x \leqq 1$ at $Rm = 50$, respectively. In Fig. 11, the solution with the original LENS undershoots slightly in the region ($0.7 \leqq x \leqq 0.8$) with strong absorption. The solution with the optimized LENS at $Rm = 50$ is in good agreement with the exact solution at the computational mesh points.

4. CONCLUSIONS

A new FVDM on finite differencing was proposed, in which the spatial difference for discretizing the convection term is optimized so that the total deviation of the numerical solution from the exact solution of the convection–diffusion equation is minimized, under the condition that roots of the characteristic equation of the resulting difference equation are always nonnegative to ensure the numerical stability.

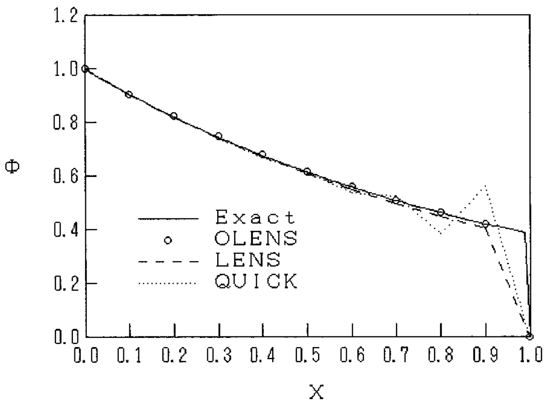

FIG. 10. Comparison of solutions with $Rm = 100$, $S = 1000$, and $Q_0 = 10$.

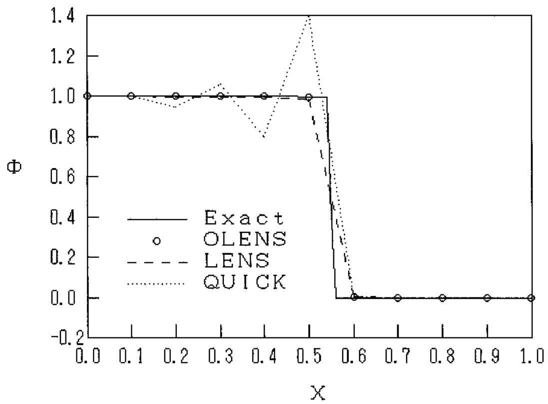

FIG. 12. Comparison of solutions with $Rm = 100$ and $S(x) = 10^6$ $(0.55 \leqq x \leqq 1)$.

The present FVDM was applied to the LENS. The optimum spatial difference of the LENS was derived in terms of mesh Reynolds numbers of up to 1000. It was found that the optimization of the LENS from the viewpoint of numerical stability and accuracy for large mesh Reynolds numbers greater than about 10 is achieved when a root of the characteristic equation for the resulting difference equation approaches its asymptote, namely when the characteristic roots have poles.

By using the optimum spatial difference the numerical accuracy of the LENS for the one-dimensional steady convection–diffusion equations was increased without numerical oscillations for all mesh Reynolds numbers.

The present study suggests that an optimum spatial difference from the viewpoint of numerical stability and accuracy exists according to the numerical schemes. Thus if the optimum spatial difference for the transport equation were to be found, we might expect to obtain highly accurate solutions free from numerical oscillations.

REFERENCES

1. M. Atias *et al., AIAA J.* **15**(2), 263 (1977).
2. B. P. Leonard, *Comput. Methods* Appl. Mech. Eng. **19,** 59 (1979).
3. J. K. Dukowicz and J. D. Ramshaw, *J. Comput. Phys.* **32,** 71 (1979).
4. B. P. Leonard, *Handbook of Numerical Heat Transfer* (Wiley, New York, 1988), p. 347.
5. T. Kawamura and K. Kuwahara, AIAA-84-0340, 1984 (unpublished).
6. S. K. Godunov, *Math. Sb.* **47,** 271 (1959).
7. J. P. Boris and D. L. Book, *J. Comput. Phys.* **11,** 38 (1973).
8. M. Chapman, *J. Comput. Phys.* **44,** 84 (1981).
9. A. Harten, *J. Comput. Phys.* **49,** 357 (1983).
10. A. Harten, *J. Comput. Phys.* **83,** 148 (1989).
11. D. N. de Allen and R. V. Southwell, *J. Mech. Appl. Math.* **8,** 129 (1955).
12. D. B. Spalding, *Int. J. Numer. Methods Eng.* **4,** 551 (1972).
13. K. Barret, *Numerical Modelling in Diffusion Convection* (Pentech, London/Plymouth, 1982), p. 33.
14. C. Günther, *Computational Techniques and Applications CTAC-87,* edited by J. Noye and C. Fletcher (Elsevier Science, Amsterdam, 1988), p. 249.
15. Cl. Günther, *Int. J. Numer. Methods Eng.* **34,** 793 (1992).
16. K. Sakai, *Comput. Fluid Dyn. J.* **1** (1), 34 (1992).
17. M. Carroll and J. J. H. Miller, *Computational and Asymptotic Methods* (Boole, Dublin, 1980), p. 225.
18. Cl. Günther, *Z. Angew. Math. Mech.* **72,** T521 (1992).
19. C. Prakash, *Numer. Heat Transfer* **7,** 165 (1984).
20. K. Sakai, *J. Nucl. Sci. Technol.* **29** (28), 824 (1992).
21. K. Sakai, *Trans. Am. Nucl. Soc.* **69,** June, 227 (1993).
22. K. Sakai, *Comput. Fluid Dyn. J.* **2**(2), 161 (1993).
23. L. Degtyarev *et al., Differential Equations* **29**(7), 1179 (1994).
24. K. Sakai, *J. At. Energy Soc. Japan* **34**(6), 544 (1992) [Japanese]